ORBIT DETERMINATION ANALYSIS FOR A JOINT UK-AUSTRALIAN SPACE SURVEILLANCE EXPERIMENT

M. Rutten,[*] T. Bessell,[*] N. Gordon,[*,†]
[*]*NSID, Defence Science and Technology Organisation, Australia*
[†]*School of ITEE, The University of Queensland, Australia*
N. M. Harwood, R. P. Donnelly, A. Ash
Air and Weapons Systems, Defence Science and Technology Laboratory, UK
J. D. Eastment, D. N. Ladd, C. J. Walden
Science and Technology Facilities Council, Chilbolton Observatory, UK
C. Smith, J. C. Bennett, I. Ritchie
Electro-Optic Space Systems, Mount Stromlo, Australia

ABSTRACT

In February 2014 the UK and Australia carried out a joint space surveillance target tracking, cueing, and sensor data fusion experiment involving the UK Science and Technology Facilities Council Chilbolton Observatory radar, the Electro Optic Systems (EOS) satellite laser-ranging (SLR) system in Australia and a small telescope operated by the Australian Defence Science and Technology Organisation (DSTO). The experiment, coordinated by the UK's Defence Science and Technology Laboratory and DSTO, was designed to explore the combination of several different, geographically separated sensors for space situational awareness. The primary goal of the experiment was to use data from the radar in the UK to generate an orbital cue to the EOS SLR. A variety of targets sizes and orbits were chosen, under the limitations of observability by both the radar and EOS SLR.

This paper examines the orbit determination techniques used to generate cues from radar and the refined orbits resulting from accumulating SLR data. The construction of tracks using data from all three sensors is explored. Analysis of the accuracy of the orbital reconstructions is made based on comparisons with the measured data and accurate ephemerides provided by the International Laser Ranging Service. The accuracy is tested against the cueing precision requirements for each sensor.

Two companion papers describe the experimental goals, execution and achievements (Harwood et. al.) and the sensor aspects of the experiment (Eastment et al.).

1. INTRODUCTION

The UK and Australia are undertaking collaborative efforts in surveillance of space, including both theoretical and experimental studies. In February 2014 the UK's Defence Science and Technology Laboratory (DSTL) and the Australian Defence Science and Technology Organisation (DSTO) coordinated a joint target tracking, cueing and sensor data fusion experiment with the UK Science and Technology Facilities Council (STFC) and Electro Optic Systems (EOS) of Australia. The experiments utilised the STFC CAMRa radar, located at the Chilbolton Observatory, southern England, an EOS optical camera and Satellite Laser Ranging (SLR) system located at Mount Stromlo near Canberra, Australia and an experimental camera owned and operated by DSTO and located at Adelaide, Australia.

This paper describes some of the orbit determination and sensor data fusion aspects of the experiment, together with analysis and investigation of the resulting orbital and cueing accuracies. This is performed using comparisons against SLR data and self-consistency checks of the resulting forward predicted cues with future sensor observations.

The paper is structured as follows: Section 2 is a short summary of the experiment, including some of the achievements and a list of the observation times for each object. Section 3 characterises each of the sensors by comparing their measurements to the precise orbital predictions available from the International Laser Ranging Service (ILRS). Section 4 describes the orbit determination techniques used by DSTL and EOS during the experiment, while Section

5 analyses the accuracy of the generated cues by comparing them to sensor measurements. The effect of including several sensors in the estimation of orbits is explored in Section 6 for three of the objects observed during the experiment. Conclusions are made in Section 7.

2. SUMMARY OF THE EXPERIMENT

As discussed in the introduction, the main aim of the experiment was to provide orbital cues from the CAMRa radar in the UK to the EOS satellite laser-ranging (SLR) system in Australia. Further information can be found in our companion paper [1]. Achievements from the experiment included

- Cueing of the EOS SLR from orbits generated from three or four passes of radar data cues (DSTL).
- Self-cueing of the CAMRa from orbits generated from radar data (DSTL).
- Cueing of the CAMRa using orbits generated from a combination of radar and SLR data (EOS).
- Cueing of the DSTO telescope using both EOS and DSTL-generated orbits.

The DSTO telescope wasn't involved in generating data for cues, but collected data for post-event analysis.

A summary of all of the observations that were made by each sensor can be found in the Appendix of this paper. While CAMRa was able to consistently observe our list of objects over the two weeks, unfortunately weather conditions during the experiment limited the number of observations being made by the EOS and DSTO systems. The objects of interest in this paper are those that were observed by at least two sensors. That subset of objects is summarized in Figure 1.

		Feb-14									
Norad Id	**Name**	**10**	**11**	**12**	**13**	**14**	**24**	**25**	**26**	**27**	**28**
12785	COSMOS-1300	R	R	R	R	R	L	R	R		
15889	COSMOS-1666	R	RR	RR	RR	R	L	R	R	OR	O
24873	IRIDIUM-921	R	R	R	R	R			O		
24965	IRIDIUM-19	R	LRR	R	R		R	R	OR		
25042	IRIDIUM-39							LRR		R	
25291	IRIDIUM-68					RR	L	RR		R	
26121	CZ-4 DEB						L	L		OR	OR
27386	ENVISAT	R	RR		RR		LRR	RR	R	RR	R
27424	AQUA			RR	R	RR	LRR		RR	R	
27597	ADEOS2	L		L				R	R	RRR	OR
28931	ALOS-1	L	RR	R		RR	LRR		RR	O	RR
32382	RADARSAT-2	R	R		R	R	R	LRR	ORR	R	R
32958	FENGYUN-3A	R			R		L	RR	RR	ORR	OR
36508	CRYOSAT-2	L	R	L			L	L		OR	
37214	FENGYUN-3B						LRR	RR	R	R	RR

Figure 1. Summary of observations made by CAMRa (R), the EOS SLR (L) and the DSTO optical system (O) where there are a total of at least four observations by at least two sites. A light grey R designates a CAMRa observation which could not contribute to orbit determination. Shaded rows correspond to the objects which have ILRS predicted ephemeris.

3. SENSOR CHARACTERISTION

For the purposes of this paper, the relevant details of the sensors involved are as follows:

- CAMRa
  - S-band (3GHz) radar, 0.5μs pulse-length, 14ms PRI
  - Located at Chilbolton in the UK
  - Cueing accuracy requirement of +/- 8.4 arc-minutes (3dB beamwidth of 0.28˚)
- EOS SLR
  - satellite laser ranging (SLR), using a 200W (average) 1.064μm laser with 5ns pulses at 100Hz
  - Located at EOS Space Systems, Mt Stromlo in Australia
  - Cueing accuracy requirement (field of view for optical acquisition) +/- 7 arc-minutes

- DSTO telescope
    - a small aperture (10 inch) f/3 telescope
    - Located at DSTO, Edinburgh in Australia
    - Cueing accuracy requirement (field of view) +/-38 arc-minutes
    - Limited to solar terminator periods (just after sunset or just before sunrise) for observation

Defining the accuracy of each sensor using their specifications may not reflect the system-level performance. We can gauge the accuracy of these sensors as systems for observing satellites, using a comparison of their measurements against objects with known location. In this work we use the precision orbital predictions on two LEO (low earth orbit) satellites available from the ILRS (International Laser Ranging Service) [2]. ILRS predictions are published on a list of objects to support ILRS activities, typically on a daily basis with forward predictions over several days. Although these are forward predictions, they are reliably precise.

Referring to Figure 1 in the previous section, CAMRa made observations against Envisat throughout the experiment and EOS made observations against Cryosat-2 throughout the experiment. Unfortunately DSTO was only able to manage one observation against an object, Cryosat-2, for which ILRS predictions are available. ILRS data was transformed into observation coordinates (azimuth, elevation and range) relative to each sensor location [2]. Light-time corrections from satellite to sensor were accounted for in the comparison. Atmospheric refraction effects are already compensated in the EOS measurements, were neglected for the radar and are unnecessary for the optical data (due to the nature of the processing chain [3]).

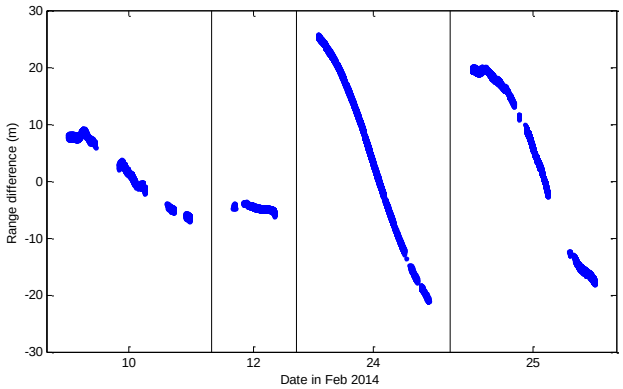

Figure 2. A comparison of the EOS observations of Cryosat-2 (36508) with ILRS predictions.

Figure 2 shows the difference between the EOS ranging measurements and predictions from the ILRS for the observations on Cryosat-2. There is a small, but significant difference between the predictions and measurements in this case, in the order of 13m RMS. It is our conclusion that these differences are primarily due to inaccuracies of the predictions, rather than the accuracy of the measurements, based on

- Similar analysis performed on the collections from geodetic satellites, Lageos-1 and Lageos-2, show differences around 0.5m RMS.
- Two agencies (HTS and ESA) both perform predictions on Cryosat-2 for the ILRS. Their predictions on LEO satellites (such as Envisat and Cryosat-2) can deviate by more than 100m over several days. The ESA predictions were used to generate Figure 2.
- Croysat-2 performed a manoeuvre between the 12th and 24th of February.

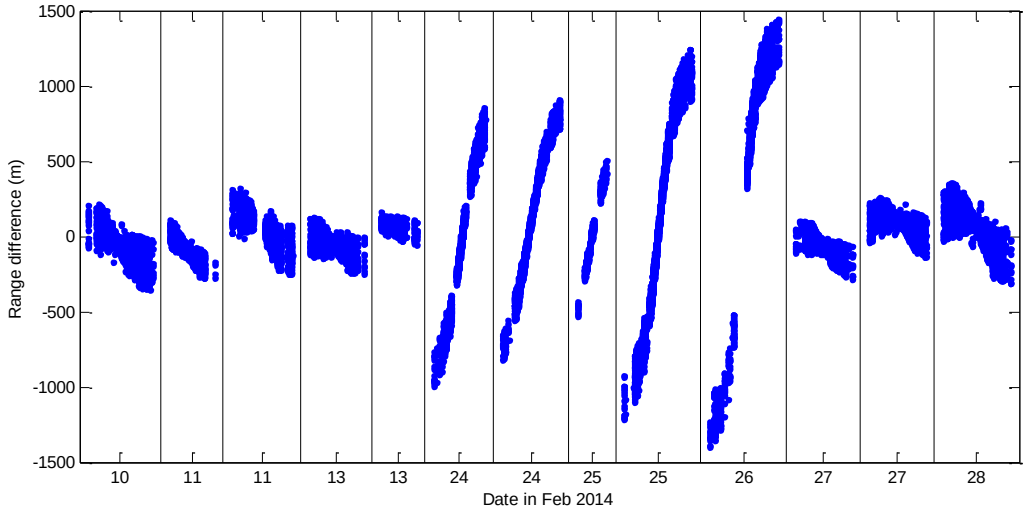

Figure 3. A comparison of the CAMRa observations of Envisat (27386) with ILRS predictions.

Figure 3 shows the difference between CAMRa-measured ranges and ILRS predictions for Envisat. The RMS error in this case is of the order of 370m. These differences are much larger than that from EOS ranging, suggesting that measurement inaccuracies (either ranging or timing) dominate the prediction errors.

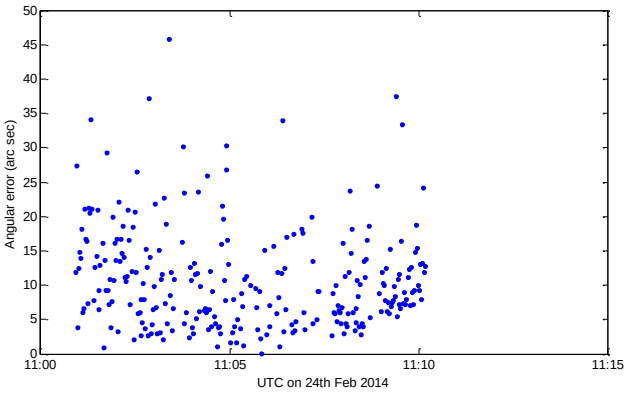

Figure 4. A comparison of the DSTO observations of Cryosat-2 (36508) with ILRS predictions.

Figure 4 shows the angular error between the ILRS predictions and DSTO observations for the single available pass of Cryosat-2 on the 24th of February. The RMS error is about 13 arc seconds. To compare with the laser and radar measurements, this corresponds to approximately 120m RMS in cross-range error. Similar to the CAMRa, these differences are dominated by measurement errors as they are much larger than we would expect from any ILRS prediction inaccuracies.

4. ORBIT DETERMINATION

Two orbit determination methods were used to generate cues during the experiment, one developed by DSTL, using CAMRa data, and one developed by EOS, using both CAMRa and SLR data. An additional method was developed at DSTO for the multi-sensor analysis in Section 6. The methods can be summarised as follows

- DSTL
  - CAMRa data only
  - EGM Earth Gravity Field Model up to degree and order 50
  - Jacchia atmospheric model

    - Third body (solar and lunar) force models
    - Three to four observed passes required for good orbit fit
- EOS
    - Combination of (loosely weighted) TLE data, EOS data and CAMRa data
- DSTO
    - Combination of CAMRa, EOS and DSTO data
    - Eigen-6s gravity model up to degree and order 10
    - Modified Harris-Priester atmospheric model
    - Third body (solar and lunar) force models

All three are differential correction methods.

The requirement for three or four radar passes to generate a cue is not arbitrary, but can be quantitavely justified through analysis of the posterior Cramer-Rao lower bound (PCRLB). The PCRLB is a lower bound on the average estimation error for a given target trajectory and sensor model, which does not depend on the type of estimator [4]. Figure 5 shows the PCRLB for a model of the CAMRa with a measurement error standard deviation of 100m. The simulated object is in LEO orbit, with an orbital period of 90 minutes and an eccentricity of 0.01. The plots compare the bound on three different orbital models accumulating four sets of measurements. The measurement times are highlighted as vertical grey bars in the plots, including the first set of measurements at the initial time. Three different propagators are compared, one which assumes a circular orbit, one which uses a 6-dimensional state of position and velocity, and one which uses a 7-dimensional state including drag coefficient with position and velocity. No prior information is used, so initial orbit determination is conducted on the first observed pass. The plots show that after one observed pass the circular propagator gives, on average, the most accurate predictions. After two and three observed passes the no-drag propagator gives the most accurate predictions and after four observed passes the inclusion of drag improves the predictions. We can see that this analytical study confirms that a model that includes drag needs, on average, at least three passes of observations to generate accurate predictions.

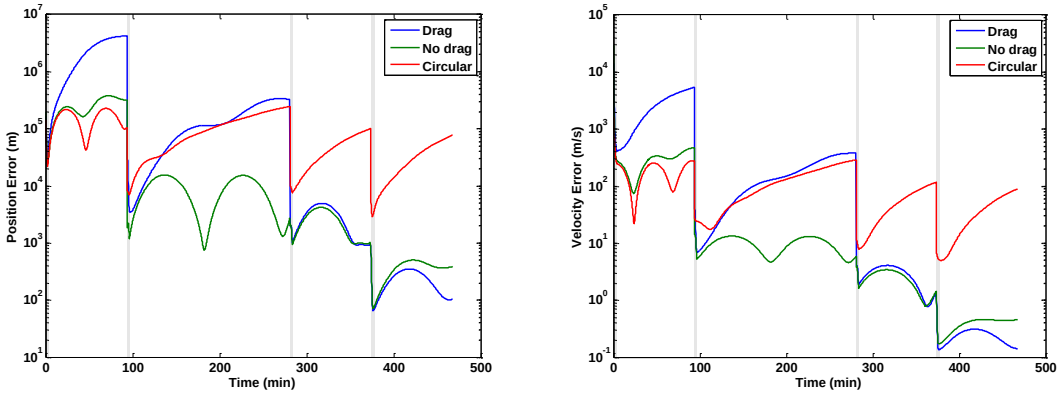

Figure 5. Posterior Cramer-Rao bound calculations, in position and velocity, for a LEO object using three different methods of propagation.

5. CUEING ACCURACIES

In order to quantify the accuracy of the cues generated by DSTL and EOS during the experiment, we compare the measured data against the most recent cue prior to the observation. The expected measurement errors for each sensor, as characterised in Section 3, are used to make a judgement about the relative accuracy of the cue. As summarised in Section 3 the cueing accuracy requirements for all three sensors are described in angles. Since both CAMRa and EOS measure range, those measurements cannot be directly related to cueing accuracy requirements, although they are useful indications of overall accuracy. On the other hand the DSTO angle measurements are appropriate for testing against cueing accuracy requirements.

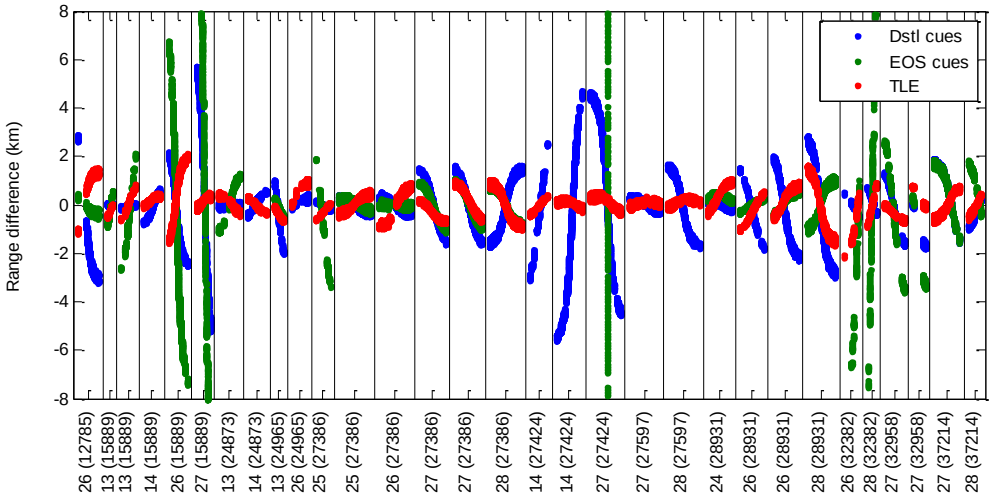

Figure 6. The difference between the CAMRa-generated cues and the CAMRa-measured range. The labels along the x-axis are the date of the observation (in Feb 2014), with the NORAD ID of the satellite in brackets.

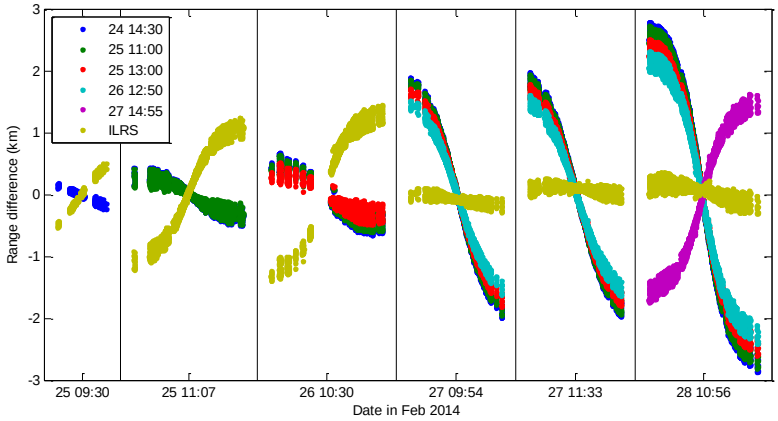

Figure 7. The difference between the CAMRa-generated cues and the CAMRa-measured range for Envisat (27386). These are compared against the results with the ILRS predictions. The labels along the x-axis are the date and time of the observation (in Feb 2014). The colours represent differences between cues made on different dates and times.

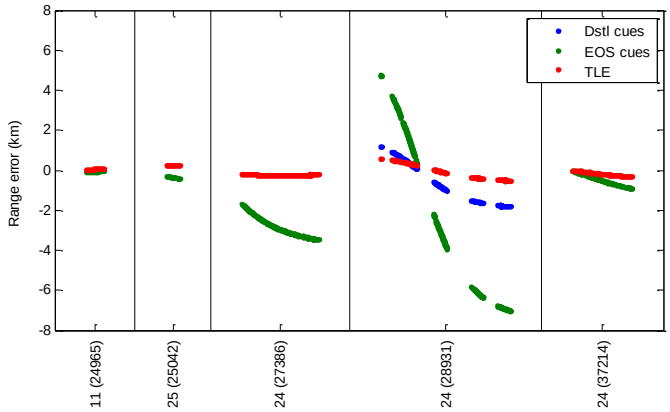

Figure 8. The difference between the Dstl and EOS-generated orbits and the EOS SLR measurements. Differences between measurements and the NORAD TLEs are shown for comparison. The labels along the x-axis are the date of the observation (in Feb 2014), with the NORAD ID of the satellite in brackets.

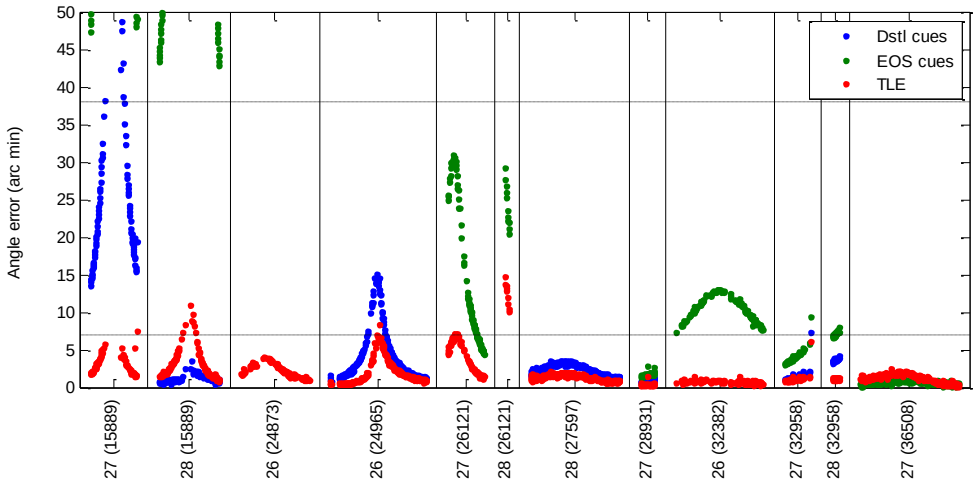

Figure 9. The angular error between the orbital predictions and the DSTO-measured angles. The labels along the x-axis are the date of the observation (in Feb 2014), with the NORAD ID of the satellite in brackets. The dotted horizontal lines are the required cueing accuracy for the EOS system (7 arc min) and the DSTO system (38 arc min).

During the experiment DSTL generated cues on 11 of the objects in Figure 1, using data from CAMRa, while EOS generated cues on all of those objects using a combination of CAMRa and TLE data. We can compare the cues generated using CAMRa data against the radar's own measurements of subsequent passes. The results are shown in Figure 6 as the difference between the measured range and the expected range from the cue. For many of the cases the errors are comparable to those measured against the ILRS predictions, suggesting sufficient accuracy of the orbit determination in those instances. The overall RMS error in range is 1.5km for the Dstl cues and 31km for the EOS cues, as compared to the 340m against ILRS predictions from Section 3. Figure 6 also shows the difference between the measurements and the NORAD TLE for the same time period. It is apparent that both the Dstl and EOS-generated cues are similar in several cases, despite using a small number of passes from single sensor. The overall RMS range error is 500m against the TLEs.

Given the large number of observations of Envisat (27386), we can compare observations against different versions of the cue as the orbit determination accumulated more data. These results, focusing on the DSTL-generated cues, are plotted in Figure 7, where we see a gradual reduction in the difference between the predicted range from the cue and the measured range. The cue generated on the 24th used 7 passes of data (from the 10th, 11th, 13th and 24th), with more being accumulated as they were observed. As a comparison, differences with the ILRS prediction are also plotted in Figure 7. For the first 3 passes the self-generated cue out-performs the ILRS prediction. While initially surprising, the results in Figure 3 suggest that there is similar timing bias on the CAMRa measurements taken on the 24th, 25th and 26th. Thus the orbit estimated from that radar data accommodates the timing bias, resulting in smaller errors compared to the ILRS predictions.

Laser ranging data from EOS was collected for five separate objects using the radar-only cue for one of these examples. A comparison between the measured ranges and predicted ranges from the cues is shown in Figure 8. For these cases the EOS-generated cues have an RMS error of 3.5km and the single DSTL cue has an RMS of 1.2km. As a comparison, the TLEs have a 290m RMS error against these measurements.

The cues generated by DSTL and EOS were used to observe 8 of the objects from Figure 1 with the DSTO telescope. Figure 9 shows the error between the measured angles and the expected angles from the cues. In all instances the DSTL-generated cues are within the field of view of the sensor (38 arc-minutes) for most of the pass. Significantly, the angular errors are within the EOS 7 arc-minute acquisition threshold for all but one of the cases. The RMS error in angle is 8.3 arc-minutes for the DSTL-generated cues. The EOS-generated cues are not as accurate in general, with an overall RMS error of 53 arc-minutes. As a comparison, the RMS error against the TLEs is 2.5 arc-minutes.

6. MULTIPLE SENSOR ORBIT DETERMINATION

While the previous section described results on the orbit determination which was performed in real time during the experiment, this section summarises analysis that has been undertaken since the event. Combinations of radar and laser ranging data that were not utilised during the experiment are combined into orbital estimates. Additionally, a combination of data from all three sensors is used to estimate an orbit. Once again, we use differences between measurements and predictions from the orbital estimate to quantify the accuracy, rather than measurement residuals from the orbital estimation.

Referring to Figure 1, there are three objects for which there were collections from all three sensors during the second week of the experiment. The times of those observations are summarised here:

Cosmos-1666 (15889)

- EOS 24 Feb 11:17
- CAMRa 25-Feb 08:37
- CAMRa 26-Feb 08:29
- CAMRa 27-Feb 08:20
- DSTO 27-Feb 10:47

CZ-4 Debris (26121)

- EOS 24-Feb 10:35
- EOS 25-Feb 10:50
- CAMRa 27-Feb 08:49
- DSTO 27-Feb 11:12
- CAMRa 28-Feb 09:03
- DSTO 28-Feb 11:26

Fengyun-3a (32958)

- EOS 24-Feb 11:26
- CAMRa 25-Feb 10:11
- CAMRa 25-Feb 11:52
- CAMRa 26-Feb 09:54
- CAMRa 26-Feb 11:34
- CAMRa 27-Feb 09:34
- CAMRa 27-Feb 11:16
- DSTO 27-Feb 12:06

For the Cosmos satellite and the Fengyun satellite, we analyse the difference between orbits generated with radar-only data and orbits generated with both radar data and the EOS observations from the 24th Feb. These results, compared against the angles measurements made on the 27th, are shown in Figure 10. We can see that in both cases the laser observations improve the orbital estimates, despite being three days before the DSTO observation. For the Cosmos the improvement is significant, such that with the laser data included the cue is within the EOS 7 arc-minute acquisition threshold. In this case it appears that three collections from CAMRa were not sufficient to generate an accurate cue. For the Fengyun both cues are well within the 7 arc-minute accuracy requirement, however the addition of the EOS data improves the cue by roughly 30 arc-seconds.

For the debris we analyse the difference between an orbit generated using a combination of laser and radar data against an orbit estimated using an additional optical observation. Four passes of ranging data (two from EOS and two from CAMRa) were used to generate one orbital estimate. A second estimate was made using the ranging data plus a single optical observation on the 27th. These are both compared against the DSTO measurements made on the 28th in Figure 10. Again we can see that both of these predictions easily meet the 7 arc-minute accuracy requirement. The addition of the optical data improves the accuracy of the predictions down to within 30 arc-seconds.

7. CONCLUSIONS

This paper has described the orbit determination and fusion aspects of an SSA experiment conducted in February 2014. The sensors involved in the experiment were the CAMRa, a radar in Southern England, the EOS satellite laser ranging system near Canberra, Australia, and an optical system at DSTO Edinburgh, Australia. The accuracy of the measurements made by each of these systems has been evaluated by comparison against precision ILRS ephemerides.

Orbital estimates were generated during the experiment to be used as cues for the other sensors. Cues were generated in real-time by DSTL using only CAMRa data and by EOS using a combination of CAMRa data, EOS SLR data and TLEs. These cues were used successfully during the experiment. This paper summarised post-event analysis of the accuracy of these cues, compared against the sensor measurements taken during the experiment. In general the accuracies compare favourably with the sensor measurement errors and cueing accuracy requirements of the three sensors.

Three examples were chosen to explore the effects of combining data from all three sensors, demonstrating the potential benefit of using multiple, heterogeneous, graphically dispersed sensors in orbital estimation.

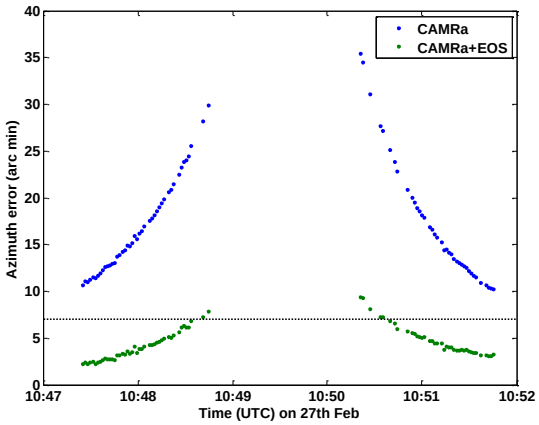

Cosmos-1666 (15889)

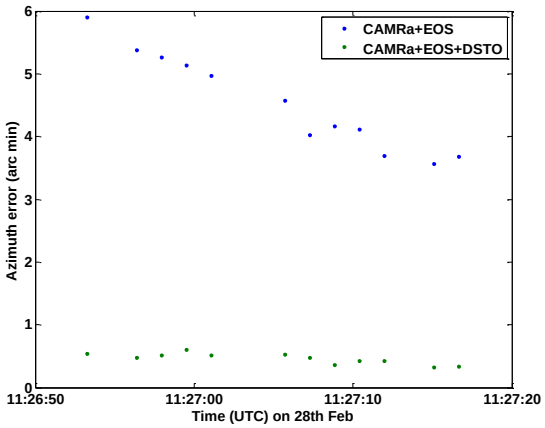

CZ-4 Debris (26121)

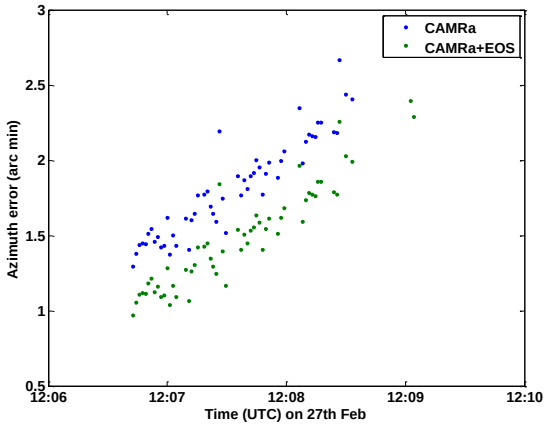

Fengyun-3a (32958)

Figure 10. Predictions as a result of orbit determinations made using a combination of data from two or three sensors. Plots show differences between the orbital prediction and the observed angles from the DSTO telescope.

8. REFERENCES

[1] N. M. Harwood et. al., "Joint UK-Australian Space Surveillance Target Tracking, Cueing and Sensor Data Fusion Experiment," in *AMOS 2014*.

[2] M. R. Pearlman, J. J. Degnan and J. M. Bosworth, "The International Laser Ranging Service," *Advances in Space Research*, vol. 30, no. 2, pp. 135-143, 2002.

[3] J. D. Eastment et. al., "Technical Description of Radar and Optical Sensors Contributing to Joint UK-Australian Satellite Tracking, Data Fusion and Cueing Experiment,," in *AMOS 2014*.

[4] J. H. Taylor, "The Cramér-Rao Estimation Error Lower Bound Computation for Deterministic Nonlinear Systems," *IEEE Transactions on Automatic Control*, Vols. AC-24, no. 2, pp. 343-344, 1979.

APPENDIX – SUMMARY OF OBSERVATIONS

Summary of the observations made by CAMRa (R), the EOS SLR (L) – where ranging data was available – and the DSTO optical system (O). A light grey R designates a CAMRa observation which could not contribute to orbit determination. Shaded rows correspond to the objects which have ILRS predicted ephemeris.

		Feb-14									
Norad Id	Name	10	11	12	13	14	24	25	26	27	28
8820	LAGEOS-1	L					L	L			
12154	COSMOS-1242						R			R	R
12785	COSMOS-1300	R	R	R	R	R	L	R	R		
13120	COSMOS-1346	R			R			R		RR	
13402	COSMOS-1400							RR		RR	
13770	COSMOS-1437	R			R	R				R	
13818	COSMOS-1441						R		R	R	
14819	COSMOS-1544	R		R		R	R				R
15889	COSMOS-1666	R	RR	RR	RR	R	L	R	R	OR	O
16908	AJISAI	R					LLL	L			
16326	COSMOS-1707	RR	RR	R	RR		R	R		R	
16986	COSMOS-1782						L			R	R
19045	COSMOS-1939							R			R
22195	LAGEOS-2						LL	L			
23710	RADARSAT		R	R	R	R		R	RR		R
24277	ADEOS	RR	R	R	RR		RR	RR		R	RR
24793	IRIDIUM-7	L	R								
24795	IRIDIUM-5			R	R						
24836	IRIDIUM-914					R			OR		
24842	IRIDIUM-911	RR			R	R				RR	
24869	IRIDIUM-15	RR	R								
24871	IRIDIUM-920						R	R		RR	R
24872	IRIDIUM-18	R	R	RR	R						
24873	IRIDIUM-921	R	R	R	R	R			O		
24903	IRIDIUM-26			R	R						
24949	IRIDIUM-30		L	LR							
24965	IRIDIUM-19	R	LRR	R	R		R	R	OR		
24968	IRIDIUM-37	LR	LR								
25041	IRIDIUM-40						R	R			
25042	IRIDIUM-39							LRR		R	
25105	IRIDIUM-24		R		R		R				
25170	IRIDIUM-56	R	R			R					
25290	IRIDIUM-67						L	R		RR	
25291	IRIDIUM-68					RR	L	RR		R	
25319	IRIDIUM-69						R				
25320	IRIDIUM-71			R			R				
25468	IRIDIUM-81		R			R					
25527	IRIDIUM-2							R			
25577	IRIDIUM-20										
25778	IRIDIUM-21	R		R	R						
26121	CZ-4 DEB						L	L		OR	OR
27372	IRIDIUM-91		L								
27374	IRIDIUM-94	R									
27386	ENVISAT	R	RR		RR		LRR	RR	R	RR	R
27392	GRACE-2	R		R	R	R			R	R	
27424	AQUA			RR	R	RR	LRR		RR	R	
27597	ADEOS2	L		L				R	R	RRR	OR
28931	ALOS-1	L	RR	R		RR	LRR		RR	O	RR
31793	SL-16 R/B							R			
32382	RADARSAT-2	R	R		R	R	R	LRR	ORR	R	R
32958	FENGYUN-3A	R			R		L	RR	RR	ORR	OR
36508	CRYOSAT-2	L	R	L			L	L		OR	
37214	FENGYUN-3B						LRR	RR	R	R	RR